A modified model of helical resonator with predictable loaded resonant frequency and Q-factor

K. Deng, Y. L. Sun, W. H. Yuan, Z. T. Xu, J. Zhang, Z. H. Lu,[a] and J. Luo
MOE Key Laboratory of Fundamental Quantities Measurement, School of Physics, Huazhong University of Science and Technology, Wuhan 430074, China

(Received 12 July 2014; accepted 27 September 2014; published online 15 October 2014)

High voltage radio frequency (RF) supply is a critical part in an ion trapping system. The RF supply should have high Q-factor and relatively high driving frequency. A frequently used RF supply for an ion trap system is a helical resonator. In certain applications, it is advantageous to have a predictable resonant frequency and Q-factor when the helical resonator is connected to a capacitive load. We develop a model to describe the behavior of a helical resonator with capacitive load. With this model, we can correctly predict the loaded resonant frequency and the loaded Q-factor. To test our prediction, we construct a helical resonator, and measure its resonant frequencies and Q-factors under different capacitive loads. The experimental results agree with our prediction. © *2014 AIP Publishing LLC*. [http://dx.doi.org/10.1063/1.4897478]

I. INTRODUCTION

For the past several decades radio frequency (RF) ion traps have found many applications in mass spectroscopy,[1] precision measurements,[2] and quantum information.[3] The main advantages of using cold ions in ion traps include longer interaction time and smaller Doppler broadening effects, making them highly suitable for research in precision spectroscopy and frequency standards. Microwave atomic clocks[4,5] and optical atomic clocks[6,7] have been built based on different ions. Ion trap is also an important tool in quantum simulation[8] and quantum information processing[9] since the external degrees of freedom of the ions can be cooled down to the vibrational ground state, and the ions feature long coherence time.

To drive an RF ion trap, we need RF power supplies that can provide the required electric potentials to confine ions. The RF power supply should feature both high RF voltage and high driving frequency. Higher RF voltages for traps mean larger trapping depths and longer trapping times.[10] A commercial RF amplifier can generate several watts of RF power. However, the amplifier and its load should be impedance matched, otherwise most of the power will be reflected back. In order to transmit as much RF power as possible into the traps, high Q-factor resonators are used to match the impedance of RF amplifiers and ion traps. Applying RF voltages via a high Q-factor resonator filters out the power in unwanted frequencies, reduces their contribution to motional heating of ions,[11] and also provides higher RF voltages per input power. In addition, high Q-factor resonator with higher resonant driving frequency is generally required in ion trap experiments where strong binding limit is required.[12] Higher driving frequency creates higher secular frequency, which makes strong binding limit and smaller Lamb-Dicke parameter easier to be achieved, and facilitates faster ions motional ground state cooling.

The high Q-factor resonator with higher resonant frequency can be realized through a helical resonator.[13] With its simple design, helical resonators have seen many applications in atomic frequency standards,[14] plasma physics,[15,16] precision measurements,[17] and metamaterial research.[18] The working principle of a helical resonator is similar to that of a coaxial resonator[12] with the coil as the core and the cylinder as the shield. The unloaded resonant frequency and the Q-factor of a helical resonator have been studied semi-empirically.[13] With proper design, the helical resonator can have rather large unloaded resonant frequency and Q-factor. However, when the helical resonator is connected to a capacitive load, like an ion trap, the resonant frequency and the Q-factor will decrease substantially.

The decrease of the helical resonator resonant frequency is due to the capacitive reactance of the ion trap and the connection wires between the trap and the helical resonator. Less effort has been made on how to predict the loaded resonant frequency when a helical resonator is attached to a capacitive load.[19] In some applications, a predictable loaded resonant frequency is very important. For example, in Sr^+ optical clocks, the micromotion-induced scalar Stark effect and time dilation shifts are of opposite sign and comparable magnitude. With proper choice of the resonant frequency, these two effects can be made to cancel each other.[7,20]

The decrease of the loaded Q-factor of a helical resonator is mainly caused by the resistance loss in the trap assembly. In addition, in the process of connecting the output of the helical resonator to the ion trap, connection joints can also introduce inductive and capacitive loads. As a consequence, the loaded Q-factor of the system becomes susceptible to the conditions of the connection joints. How to maintain a high loaded Q-factor proves to be challenging.

Recently, Siverns *et al.*[21] presented a lumped element equivalent circuit model to predict the loaded resonant frequency and the loaded Q-factor of a helical resonator. In this work, we present a modified lumped element equivalent circuit model that predicts the loaded resonant frequency and

[a]Electronic mail: zehuanglu@mail.hust.edu.cn.

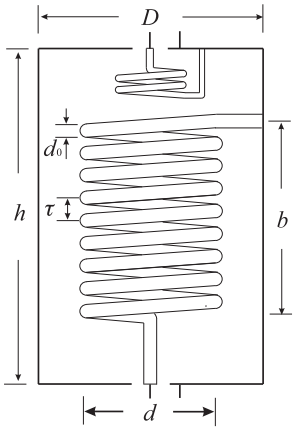

FIG. 1. Schematic diagram of a helical resonator indicating shield diameter D, shield height h, coil diameter d, coil height b, winding pitch τ, and coil wire diameter d_0.

the loaded Q-factor more accurately. We construct a helical resonator and experimentally measure the resonant frequencies and Q-factors under different loads to confirm our predictions. We use the constructed helical resonator to drive a linear ion trap to test its practical performance. We also investigate methods to achieve the highest possible loaded Q-factor for an ion trap system.

II. THEORETICAL MODEL

Figure 1 shows the schematic diagram of a helical resonator. A helical resonator consists of a copper can and two copper coils inside. The copper can acts as a shield. One smaller coil is called antenna coil. It is used to inductively couple the RF amplifier output to the helical resonator, so that the helical resonator is decoupled from the resistive output impedance of the RF amplifier. It is attached to one of the end caps in the copper can. The other coil is the main helical coil, which supplies high voltage RF signal to the ion trap. The main helical coil is attached to the other end cap of the copper can. Both coils are placed centrally in the copper can. By altering the physical properties of the antenna coil, impedance matching between the helical resonator and the RF amplifier can be achieved.

The main relevant parameters of a helical resonator include shield diameter D, shield height h, coil diameter d, coil height b, winding pitch τ, and coil wire diameter d_0, as shown in Fig. 1. In the following calculations, they are all in units of meter. To realize an optimal resonance, these parameters can be chosen according to the semi-empirical study of Macalpine and Schildknecht.[13]

To predict the resonant frequency of a combined system, Figure 2 shows a lumped element circuit to model the helical resonator with its connected load. In Fig. 2, L_a is the antenna coil self inductance, L_h is the helical coil self inductance, Z_0 is the output impedance of the RF amplifier, R_h is the helical coil resistance, R_j is the helical coil to shield connection resistance, $R_c = R_{c1} + R_{c2}$ is the contact resistance introduced by the connection between the helical resonator and the load. We found that its effect has to be separated into two parts, with R_{c1} inside the helical resonator and R_{c2} outside the resonator.

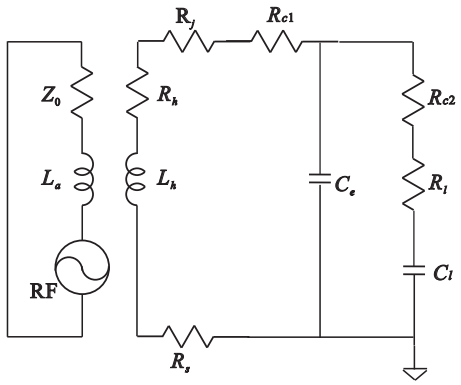

FIG. 2. Lump element circuit model of a helical resonator with its connected load. L_a is the antenna coil self inductance, Z_0 is the RF voltage source impedance, R_h is the helical coil resistance, L_h is the helical coil self inductance, R_j is the helical coil to shield junction resistance, R_{c1} and R_{c2} is the contact resistance introduced by the connection between the helical resonator and the load, R_s is the shield resistance, C_e is the equivalent capacitance of the resonator without load, C_l is the capacitance of the load, R_l is the load resistance.

R_s is the shield resistance, R_l is the load resistance, C_e is the equivalent capacitance of the helical resonator without load, and C_l is the load capacitance.

According to the RLC circuit resonant frequency definition, we have

$$f_0 = \frac{1}{2\pi\sqrt{C_e L_h}}, \tag{1a}$$

$$f_l = \frac{1}{2\pi\sqrt{(C_e + C_l)L_h}}. \tag{1b}$$

Here f_0 is the unloaded resonant frequency. The loaded resonant frequency f_l of the whole system can then be expressed as

$$f_l = \sqrt{\frac{C_e}{C_e + C_l}}\, f_0. \tag{2}$$

From Eq. (2), it can be seen that if the load capacitance C_l is much smaller than C_e, the resonant frequency will not change considerably when a load is connected to a helical resonator. If the load capacitance is not negligible, the resonant frequency will decrease appreciably.

In the model of Siverns *et al.*,[21] the equivalent capacitance of the helical resonator is represented by parallel connection of C_s and C_c, where C_c is the helical coil self capacitance, and C_s is the capacitance of the helical coil to the surrounding shield. The values of C_c and C_s can be calculated from the empirical formula, where C_c is given by[21]

$$C_c \approx \left(0.1126\frac{b}{d} + 0.08 + \frac{0.27}{\sqrt{\frac{b}{d}}}\right) d \times 10^{-10}, \tag{3}$$

and C_s is given by[21]

$$C_s \approx 39.37 b \frac{0.75}{\log\left(\frac{D}{d}\right)} \times 10^{-12}. \tag{4}$$

The equivalent capacitance of the helical resonator is then simply $C_e = C_s + C_c$.

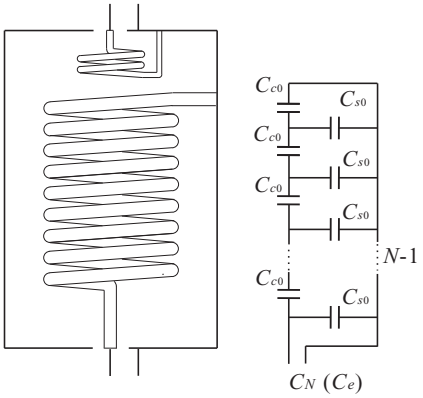

FIG. 3. Diagram showing how to calculate the equivalent capacitance C_e. C_{c0} is the self-capacitance of one turn of the helical coil, and C_{s0} is the capacitance between one turn of the helical coil wire and the surrounding shield.

Considering the structure of the helical resonator, it is apparent that this model does not consider the inter-coupling effect of C_c and C_s, therefore it does not describe the full picture. Here we use a modified model to calculate the value of C_e. When C_c and C_s are combined to give C_e, it is not a simple relationship of parallel connection or series connection. Figure 3 shows how the equivalent capacitance C_e can be composed from C_s and C_c in our model. We designate C_N as the equivalent capacitance for N winding turns. From Fig. 3, the value of C_e can be calculated by the following equations:

$$C_{c0} = (N-1)C_c, \tag{5a}$$

$$C_{s0} = C_s/(N-1), \tag{5b}$$

$$C_1 = C_{c0} + C_{s0}, \tag{5c}$$

$$C_e = C_N = \frac{1}{\frac{1}{C_{N-1}} + \frac{1}{C_{c0}}} + C_{s0}, \ N > 1. \tag{5d}$$

Here C_{c0} is the self-capacitance of one turn of the helical coil, and C_{s0} is the capacitance between one turn of the helical coil wire and the surrounding shield. The resonant frequency of the loaded system can then be calculated from Eqs. (2)–(5).

The Q-factor is defined by the amount of power stored in the resonator divided by the energy losses per cycle. From Fig. 2 and the RLC circuit model, the Q-factor can be derived as

$$Q = \frac{1}{R}\sqrt{\frac{L}{C}} = \frac{1}{R}\sqrt{\frac{L_h}{C_e + C_l}}. \tag{6}$$

Since helical coils have low self capacitances and low resistances, R can be derived as[21]

$$\begin{aligned} R &= R_h + R_j + R_s + R_{c1} \\ &\quad + \mathrm{Re}\left[\left(\frac{1}{\frac{i}{C_l\omega} + R_l + R_{c2}} + \frac{1}{\frac{i}{C_e\omega}}\right)^{-1}\right] \\ &= R_h + R_j + R_s + R_{c1} + \frac{(R_l + R_{c2})\left(\frac{1}{\omega C_e}\right)^2}{R_l^2 + \left(\frac{1}{\omega C_e} + \frac{1}{\omega C_l}\right)^2}. \end{aligned} \tag{7}$$

Since the loads normally have low resistances, R can be approximated as

$$R \approx R_h + R_j + R_s + R_{c1} + (R_l + R_{c2})\left(\frac{C_l}{C_l + C_e}\right)^2. \tag{8}$$

From the above derivation, we can predict both the resonant frequency and the Q-factor when the helical resonator is connected to a capacitive load.

III. HELICAL RESONATOR CONSTRUCTION

We construct a helical resonator to verify our prediction. In general, larger helical resonator has larger Q-factor because the stored energy is proportional to the volume and losses are proportional to the surface area, the overall Q-factor is roughly proportional to the diameter of the resonator. In order to keep the whole system compact, we select D to be 107 mm, and we design the unloaded resonant frequency f_0 to be 50 MHz. Then N should be about 9 according to the empirical study. Since the copper coil diameter d should be in the range such that $0.45 < d/D < 0.6$, we choose it to be 58 mm. The axial length of the coil b should be restricted in such a way that $b/d > 1$, we choose it to be $b = 87.5$ mm. Furthermore, lengths for the shield should be $h = b + D/2 = 141$ mm. The winding pitch is given by $\tau = b/N = 9.7$ mm. The ratio b/d determines the valid range of the copper wire diameter d_0 should be $0.4 < d_0/\tau < 0.6$, we choose d_0 to be 6 mm. Since the copper wire size is quite large, we expect the helical structure to be rigid enough so that it is not susceptible to mechanical vibrations. Diameter of the antenna coil is half of that of the helical coil, and the antenna coil is generally winded into 2–3 turns.

The resonator is constructed with the above chosen parameters. A picture of the constructed resonator is shown in Fig. 4. The antenna coil is hand-winded with 2 mm diameter copper wire. The turns and the diameter of the antenna coil can be adjusted to obtain a desired impedance matching between the helical resonator and the 50 Ω output impedance of the RF amplifier.

The main helical coil has a wire diameter of 6 mm. Since it is very important to maintain the winding pitch and the coil

FIG. 4. Picture of the constructed helical resonator. The shield diameter is 107 mm. The antenna coil has 2 turns and the main helical coil has 9 turns.

diameter to be constant, we use a lathe and a holding tube to wind the coil. First we fabricate a holding tube with an outside diameter of $d - d_0$ and a length longer than b, and then we wind the coil onto this holding tube with a lathe. Using this method, the error of the winding pitch is less than ± 0.2 mm, and the error of the coil diameter is less than ± 1 mm.

It is hard to directly solder the 6 mm coil to the shield. We attach the main helical coil to the shield by soldering it onto one end of a BNC connector. This BNC connector is mechanically mounted to the shield. A BNC short is connected to the other end of the BNC connector, which is at the outside of the shield. In order to minimize the coil to shied capacitance, the coil is placed centrally inside the shield.

In order to obtain good coupling between the antenna coil and the main coil, the distance between them is designed to be adjustable. This is realized by making matching threads on the top end cap (to which the antenna coil is attached) and the shield. Turning the top end cap changes the distance between the two coils. This adjustment helps us to obtain a very good impedance matching between the RF amplifier and the helical resonator.

IV. EXPERIMENTAL RESULTS

To test our model, we use different capacitive loads and measure the resonant frequencies as well as the Q-factors when these loads are connected to the resonator. The loads should have similar characteristics to that of ion traps. Therefore several different length coaxial cables are used as the load of the helical resonator. The capacitance increases linearly with the length of the coaxial cable. The coefficient is roughly 110 pF/m from the experimental result measured by an LCR meter (Agilent 4285A).

The cables we used are not pure capacitive loads. In order to calculate the loaded Q-factor we need to know their resistances. We can calculate the resistance of these cables first. The copper core has a diameter of $d_i = 9(1) \times 10^{-4}$ m. The resistivity of copper is $\rho = 1.68 \times 10^{-8}$ Ω m. Due to the skin effect,[22] the skin depth of copper is $\delta = 66 \times 10^{-6}/\sqrt{f}$ where the unit of frequency f is MHz and the unit of δ is meter. Since the operating frequency is in the range of tens of MHz, the contribution of the DC resistance is negligible, and we also neglect the dielectric loss of the cables.[23] It is apparent that the cable resistance is proportional to the length of the cable. Therefore the resistance of the copper core with length l is $\rho l/(\pi d_i \delta) = 0.09(1)\sqrt{f}l$. Here the unit of l is meter. The cable outer shield has an inner diameter of $d_o = 3.0(2) \times 10^{-3}$ m. Since it is made of woven copper, we give an adjustment factor of 1.3 to its resistance. The resistance of the woven copper shield is then calculated to be $1.4 \times \rho l/(\pi d_o \delta) = 0.039(9)\sqrt{f}l$. Therefore the total resistance of the cable is calculated to be $0.129(19)\sqrt{f}l$.

We can also measure the resistance of these cables directly with our LCR meter. During the measurement, one end of the cable is connected to the LCR meter and the other end of the cable is shorted by a BNC short. Figure 5 shows the resistance of cables with different lengths as a function of frequency. All of these curves can be fitted with

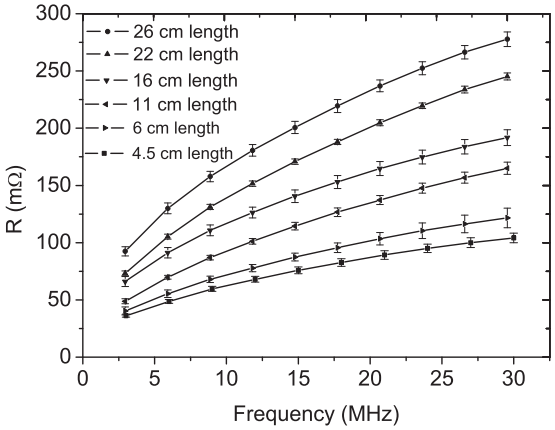

FIG. 5. The measured resistance of the cable as a function of frequency. Each data curve corresponds to cable length of 4.5 cm, 6 cm, 11 cm, 16 cm, 22 cm, and 26 cm, respectively.

$$R_l = (A + kl)\sqrt{f}. \tag{9}$$

Here A is a constant introduced by the end of the cable together with the BNC short since both the end of the cable and the BNC short is not counted in the cable length. k is a proportional coefficient, l is the length of the coaxial cable. According to these curves the coefficient k is fitted to be 0.143(4) Ω/m(MHz)$^{0.5}$, which is consistent with our theoretical calculation. The constant A is fitted to be 0.014(1) Ω/(MHz)$^{0.5}$.

Figure 6(a) shows the experimental setup for measuring the resonant frequency and the Q-factor of the helical resonator. We use a network analyzer (Agilent E5061B) to measure the resonant frequency and to calculate the Q-factor. The network analyzer is operated under the S11 mode. In this mode the device measures the ratio of the reflected power to the incident power. The resonant frequency can be directly read out from the network analyzer. The Q-factor can be calculated by dividing the resonant frequency by full-width-half-maximum (FWHM) of the resonance line. A typical measurement result is shown in Fig. 6(b).

Figure 7 shows a plot of the resonance frequency as a function of load capacitance. We are interested in capacitance range from 5 pF to 50 pF since this is the typical range over which a normally used ion trap capacitance can vary. Each data point of resonant frequency is an average of three measurements, and the error bars represent one standard deviation. Red solid curve is our theoretical prediction, and blue dashed curve is the prediction of Ref. 20. For the parameter of the helical resonator described here, C_c (self capacitance of helical coil) is 2.7 pF and C_s (capacitance of helical coil to the surrounding shield) is 9.7 pF according to Eqs. (3) and (4). Therefore the equivalent capacitance C_e in Siverns model is sum of C_c and C_s, which is 12.4 pF. This value is used to plot the blue dashed curve in Fig. 7. The equivalent capacitance C_e in our model is calculated to be 6.0 pF according to Eqs. (5a)–(5d). This value is used to plot the red solid curve in Fig. 7. Figure 7 shows that with equivalent capacitance C_e of 6.0 pF the experimental result of resonant frequency agrees with the calculation better. It can be seen that the resonance frequency

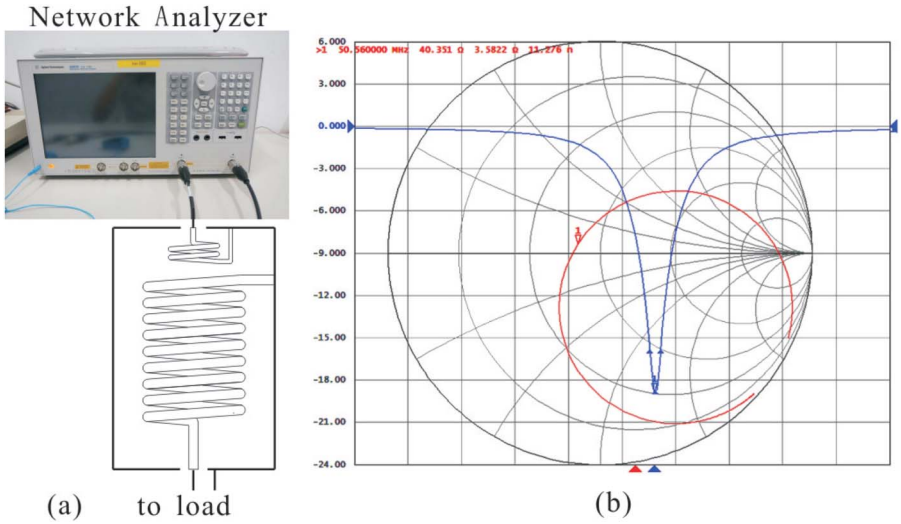

FIG. 6. (a) Experimental setup for measuring the resonant frequency and the Q-factor of the helical resonator. The network analyzer is operated under S11 mode. (b) A typical figure taken from the network analyzer showing S11 values as a function of the scanned RF frequency, from which the resonant frequency and the Q-factor can be obtained.

decreases as the load capacitance increases, and the relationship between the resonant frequency and the load capacitance fits our prediction very well. For a trap capacitance of 25 pF, the resonant frequency is half of the unloaded resonant frequency.

We also measure the Q-factor of the helical resonator under different loads. The experimental results are shown in Fig. 8. For a given load capacitance, its Q-factor is obtained after we optimize the coupling of the antenna coil and the main coil to achieve good impedance matching. Each data point of Q-factor is an average of three measurements, and the error bars represent one standard deviation.

To fit the result with our model, Eq. (8), we note that all the resistance terms are proportional to the square root of frequency due to the skin effect. We first measure the unloaded Q, which is 650(20), to derive the value of $R_h + R_j + R_s$ to be 0.89(3) Ω at frequency of 50 MHz. Therefore $R_h + R_j + R_s$ at frequency f is $0.126(4)\sqrt{f}$.

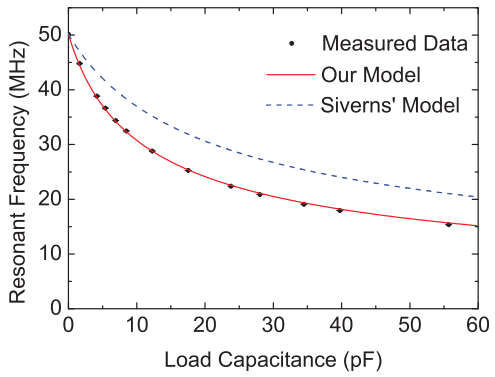

FIG. 7. The loaded resonant frequency of the helical resonator as a function of load capacitance. Each data point of resonant frequency is an average of three measurements, and the error bars represent one standard deviation. The red solid curve is our model prediction. The blue dash curve is the prediction by Siverns *et al.*[21] The unloaded resonant frequency corresponds to the designed value of 50 MHz.

Then for the $R_{ci}(i = 1, 2)$, we assume

$$R_{ci} = k_i\sqrt{f}. \tag{10}$$

Since it is difficult to directly calculate k_1 and k_2, we used measured loaded Q-factors and nonlinear least-squares-fitting of Eqs. (6) and (8) to obtain them. In Eq. (8) the value of L_h is measured by the LCR meter to be 2.0 μH. The fitted k_1 is 0.054(9) Ω/(MHz)$^{0.5}$ and k_2 is 0.22(2) Ω/(MHz)$^{0.5}$. The sum

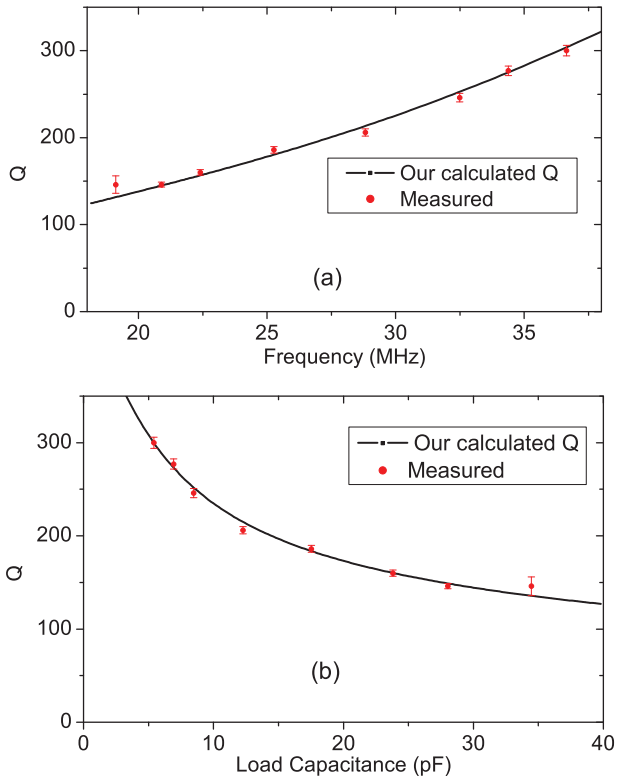

FIG. 8. The loaded Q-factor of the helical resonator as a function of (a) frequency and (b) load capacitance. Each data point of Q-factor is an average of three measurements, and the error bars represent one standard deviation.

of these two values is much larger than R_j. This is surprising since R_j also has contact resistance contribution. We do not have a definite answer for this. One possible explanation is that the contact is not pure Ohmic contact, and the contact resistance has larger value at higher voltage. Since the connection between the resonator and the load has higher voltage in comparison to that of the connection between the resonator and the BNC short, the contact resistance R_c is much larger than R_j.

With the values of k_1 and k_2 known, we can plot the predicted Q-factor as a function of load capacitances. This is shown as red solid curve in Fig. 8(b). It can be seen that the Q-factor decreases when the load capacitance increases, and the experimental result agrees with our prediction well. We also plot the Q-factor as a function of frequency as shown in Fig. 8(a).

To test the practical performance of the helical resonator, we use the helical resonator to drive a linear Paul trap. The resonator is connected directly with a vacuum feed-through. Two aluminum wires are used to connect the vacuum feed-through to the trap electrodes. The aluminum wires should be as short as possible to reduce the total capacitance of the load. The resonant frequency and the Q-factor of the helical resonator are measured before we put the trap inside vacuum chamber. After putting the trap inside the vacuum chamber, the Q-factor decreases due to the contact resistance between the connection wires and the trap electrodes. To solve the problem, we squeeze a thin layer of indium film into the junction between the trap electrodes and the connection wires to lower the contact resistance, and to increase the Q-factor. The Q-factor of the resonator is measured to be about 300 after the trap is connected.

We used the linear ion trap to trap magnesium ions as logic ions for an aluminum ion optical clock experiment. Our linear trap consists of four blade electrodes and two end-cap electrodes. This structure allows a more open optical access for cooling laser, detection laser, and fluorescence collection. All the electrodes are made of titanium. The two opposing blade electrodes are connected to the helical resonator and the other two are grounded. The distance between the two opposing blade electrodes is $2r = 1.6$ mm. The distance between the two end-cap electrodes is $2z = 3.0$ mm. The trap electrodes are hold by machinable ceramic to maintain their relative positions. The machinable ceramic is mounted on a titanium holder, which is installed in the center of a vacuum chamber. The chamber is made of titanium and had fused silica windows to allow the passage of UV laser beams. An ion pump and a titanium sublimation pump are used to maintain the UHV environment. The pressure in the vacuum chamber is about 2×10^{-8} Pa. The laser fluorescence of the trapped ions is collected by two sets of imaging lens systems, one for a photon counting module, and the other for an electron-multiplying CCD (EMCCD).

A 25 MHz RF drive is applied to the blade electrodes through the helical resonator. The RF source is a signal generator (Rhode-Schwarz SMB100A), which is further amplified by an RF amplifier (Minicircuits TIA-1000-1R8-2). The injection power into the helical resonator as well as the reflection power are measured by an RF power meter (Rhode-Schwarz NRT), which is connected between the RF amplifier and the helical resonator. In the following ion trap experiment the injection power is 0.5 W and the reflection power is 0.04 W.

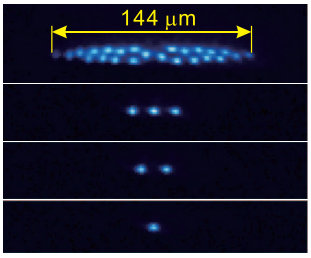

FIG. 9. Pictures of trapped and crystallized Mg^+ ions.

In the experiment, magnesium atoms are obtained by heating a magnesium oven for several minutes. In the meantime, a 285 nm fourth-harmonic-generation (FHG) laser from Toptica is used to photo-ionize the magnesium atoms. A 280 nm FHG laser from Toptica is used to laser cool and detect the trapped magnesium ions. Pictures of trapped and crystallized Mg^+ are recorded by an EMCCD camera (Andor DU-897D-CS0-UVB). The result is shown in Fig. 9, demonstrating proper operation of the constructed helical resonator.

V. DISCUSSION AND CONCLUSION

The loaded resonant frequency of a helical resonator decreases rapidly with load capacitance. To maintain a high loaded resonant frequency, it is important to have a low load capacitance, and at the same time keep the capacitance values from connectors and connection wires to a minimum. The loaded Q-factor of a helical resonator decreases rapidly with the loaded capacitance and resistance. To have high loaded Q-factor, in addition to the requirement of low load capacitance, it is very important to have small load resistance, contact resistance, and resonator resistance.

The resonator resistance can vary over the time due to the oxidation of the copper shield surface. The oxidation of the resonator will lower the Q-factor of the system. Therefore it is difficult to maintain a constant high Q-factor in long term operation. To improve the long term stability of the helical resonator, one common solution is to silver-plate the copper shield, and use silver-plated copper wire for helical coil.

The designed helical resonator and its modification not only can be used in ion trapping or ion guiding experiments, but also in any applications requiring a high voltage drive of a capacitive load, for example, in a resonant Electro-optic modulator (EOM) drive.

In conclusion, we develop a model to describe the behavior of a helical resonator with capacitive load. With this model, we can correctly predict the loaded resonant frequency and the loaded Q-factor. We construct a helical resonator, and measure its resonant frequency and Q-factor under different loads. The experimental results agree with our prediction. We also demonstrate that by optimizing the coupling between the antenna coil and main coil, and by decreasing the contact resistance between the helical resonator and the ion trap, it is

possible to substantially increase the Q-factor of the helical resonator.

ACKNOWLEDGMENTS

We wish to thank the help of H. Guan and K. L. Gao in the construction of our helical resonator. The project is partially supported by the National Basic Research Program of China (Grant No. 2012CB821300), the National Natural Science Foundation of China (Grant Nos. 11304109, 11174095, and 61108025), Specialized Research Fund for the Doctoral Program of Higher Education, and Program for New Century Excellent Talents by the Ministry of Education.

[1]D. J. Douglas, A. J. Frank, and D. Mao, "Linear ion traps in mass spectrometry," Mass Spectrom. Rev. **24**, 1 (2005).
[2]J. P. Karr, "Precision measurements with non-laser-cooled trapped ions," J. Phys. B **42**, 154018 (2009).
[3]H. Häffner, C. F. Roos, and R. Blatt, "Quantum computing with trapped ions," Phys. Rep. **469**, 155 (2008).
[4]E. A. Burt, S. Taghavi-Larigani, and R. L. Tjoelker, "High-resolution spectroscopy of $^{201}Hg^{+}$ hyperfine structure: A sensitive probe of nuclear structure and the hyperfine anomaly," Phys. Rev. A **79**, 062506 (2009).
[5]J. W. Zhang, Z. B. Wang, S. G. Wang, K. Miao, B. Wang, and L. J. Wang, "High-resolution laser microwave double-resonance spectroscopy of hyperfine splitting of trapped $^{113}Cd^{+}$ and $^{111}Cd^{+}$ ions," Phys. Rev. A **86**, 022523 (2012).
[6]C. W. Chou, D. B. Hume, J. C. J. Koelemeij, D. J. Wineland, and T. Rosenband, "Frequency comparison of two high-accuracy Al^{+} optical clocks," Phys. Rev. Lett. **104**, 070802 (2010).
[7]A. A. Madej, P. Dubé, Z. Zhou, J. E. Bernard, and M. Gertsvolf, "$^{88}Sr^{+}$ 445-THz single-ion reference at the 10^{-17} level via control and cancellation of systematic uncertainties and its measurement against the SI second," Phys. Rev. Lett. **109**, 203002 (2012).
[8]C. Schneider, D. Porras, and T. Schaetz, "Experimental quantum simulations of many-body physics with trapped ions," Rep. Prog. Phys. **75**, 024401 (2012).
[9]D. J. Wineland and D. Leibfried, "Quantum information processing and metrology with trapped ions," Laser Phys. Lett. **8**, 175 (2011).
[10]W. Paul, "Electromagnetic traps for charged and neutral particles," Rev. Mod. Phys. **62**, 531 (1990).
[11]Q. A. Turchette, D. Kielpinski, B. E. King, D. Leibfried, D. M. Meekhof, C. J. Myatt, M. A. Rowe, C. A. Sackett, C. S. Wood, W. M. Itano, C. Monroe, and D. J. Wineland, "Heating of trapped ions from the quantum ground state," Phys. Rev. A **61**, 063418 (2000).
[12]S. R. Jefferts, C. Monroe, E. W. Bell, and D. J. Wineland, "Coaxial-resonator-driven rf (Paul) trap for strong confinement," Phys. Rev. A **51**, 3112 (1995).
[13]W. W. Macalpine and R. O. Schildknecht, "Coaxial resonators with helical inner conductor," Proc. IRE **47**, 2099 (1959).
[14]J. H. Yang, Y. Zhang, X. M. Li, and L. Li, "An improved helical resonator design for rubidium atomic frequency standards," IEEE Trans. Instrum. Meas. **59**, 1678 (2010).
[15]P. Bletzinger, "Dual mode operation of a helical resonator discharge," Rev. Sci. Instrum. **65**, 2975 (1994).
[16]K. Niazi, A. J. Lichtenberg, and M. A. Lieberman, "The dispersion and matching characteristics of the helical resonator plasma source," IEEE Trans. Plasma Sci. **23**, 833 (1995).
[17]R. J. Deri, "Dielectric measurements with helical resonators," Rev. Sci. Instrum. **57**, 82 (1986).
[18]J. W. Zhu, T. Hao, C. J. Stevens, and D. J. Edwards, "Optimal design of miniaturized thin-film helical resonators," Appl. Phys. Lett. **93**, 234105 (2008).
[19]R. F. Welton, E. W. Thomas, R. K. Feeney, and T. F. Moran, "Simple method to calculate the operating frequency of a helical resonator-RF discharge tube configuration," Meas. Sci. Technol. **2**, 242 (1991).
[20]P. Dubé, A. A. Madej, M. Tibbo, and J. E. Bernard, "High-Accuracy measurement of the differential scalar polarizability of a $^{88}Sr^{+}$ clock using the time-dilation effect," Phys. Rev. Lett. **112**, 173002 (2014).
[21]J. D. Siverns, L. R. Simkins, S. Weidt, and W. K. Hensinger, "On the application of radio frequency voltages to ion traps via helical resonators," Appl. Phys. B **107**, 921 (2012).
[22]H. T. Kohlhaas and F. J. Mann, *Reference Data for Radio Engineers*, 2nd ed. (Federal Telephone and Radio Corporation, New York, 1946).
[23]R. F. Eaton and C. J. Kmiec, "Electrical losses in coaxial cable," in *Proceedings of the 57th International Wire & Cable Symposium* (IWCS, Inc., 2008), p. 515.